

Friedel-Crafts Reaction: Theoretical Study of the Mechanism of Benzene Alkylation with Isopropyl Chloride Catalyzed by AlCl_3 and Al_2Cl_6

Isac C. Nogueira^a and Josefredo R. Pliego Jr. *,^a

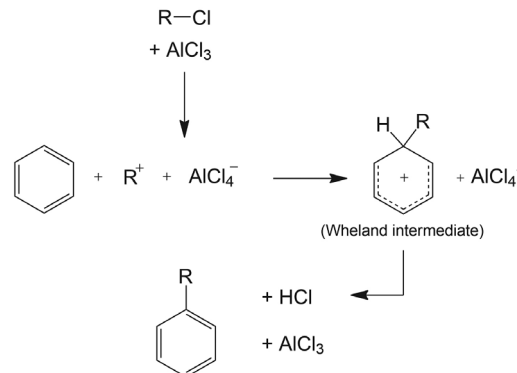
^aDepartamento de Ciências Naturais, Universidade Federal de São João Del Rei, 6301-160 São João Del Rei-MG, Brazil

The classical alkylation reaction of benzene with isopropyl chloride catalyzed by the species AlCl_3 and Al_2Cl_6 was studied using reliable calculations at M06-2X/def2-TZVPP//X3LYP/def2/SVP level of theory and SMD model for solvent effect. We evaluated the formation of dimers, trimers, tetramers, and pentamers and showed that Al_2Cl_6 dimers exist in greater proportion, in agreement with experimental observations. The experimental solubility of Al_2Cl_6 in benzene was also included in the theoretical kinetics analysis. The reaction catalyzed by AlCl_3 species presents the highest barrier, in part due to unfavorable dissociation of the Al_2Cl_6 species. The mechanism via Al_2Cl_6 catalysis is more effective and even considering its low solubility, the calculated observed ΔG^\ddagger is only 20.6 kcal mol⁻¹, indicating a fast reaction rate. The mechanism involves the formation of the $\text{CH}_3\text{CHCH}_3^+ \dots \text{Al}_2\text{Cl}_7^-$ ion pair, which reacts with benzene to form a Wheland intermediate and this carbon-carbon bond formation step corresponds to the rate-determining one.

Keywords: electrophilic aromatic substitution, Lewis acid, free energy profile, microkinetic analysis, solvent effects, ion pairing

Introduction

A relevant step in organic synthesis is the formation of carbon-carbon bonds.¹⁻⁴ This allows the generation of molecules of high added value, having a centuries-old history in synthetic organic chemistry.¹⁻⁴ The Friedel-Crafts reaction, developed by Charles Friedel and James Crafts in 1877, has an important application in this sense, mainly for the alkylation and acylation of aromatic compounds.¹⁻⁶ In the case of alkylation, the methodology consists of using a Lewis acid, such as AlCl_3 , to activate the alkyl halide (RX), forming an active intermediate (R^+ or $\text{R-X} \dots \text{AlCl}_3$) able to promote an electrophilic substitution reaction with the aromatic compound.^{1,2,5,6} The reaction involves the Wheland or σ intermediate, which loses a proton, leading to the formation of the alkylated product and regeneration of the catalyst.^{1,2,5} This process is depicted in Scheme 1 for the benzene alkylation reaction catalyzed by AlCl_3 . It is interesting to note that several catalysts for Friedel-Crafts reactions have been developed and, in particular, in the 1980s, the first asymmetric catalysts appeared.⁷⁻⁹ This kind of methodology has been used in applications from petroleum chemistry to drug synthesis.^{3,6}



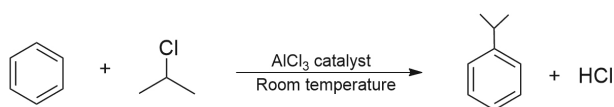
Scheme 1. Usual mechanism of Lewis acid-catalyzed alkylation of benzene found in textbooks.

Although the Friedel-Crafts reaction is practical and very useful, some aspects make your application limited, especially with classical catalysts such as AlCl_3 . For example, AlCl_3 leads to isomerization of primary alkyl halides, resulting in different isomers in the product.^{10,11} Furthermore, this methodology often leads to polyalkylation and highly unwanted mixture of products.^{1-3,5,6} Another unfavorable point is that AlCl_3 can often form complexes with reactants and products, requiring the use of stoichiometric amounts of the catalyst.⁶ Such limitations and the importance of this reaction have induced recent researches on this reaction class.¹²⁻¹⁵

*e-mail: pliego@ufsj.edu.br

Editor handled this article: José Walkimar M. Carneiro

Some theoretical studies have explored the interactions between the catalyst and the reactants of the Friedel-Crafts reactions.¹⁶⁻¹⁸ Mechanistic studies of Friedel-Crafts alkylation, acylation and similar reactions via computational methods have also been reported.¹⁹⁻²⁶ In particular, the mechanism of the Friedel-Crafts alkylation is not as simple as the Scheme 1 suggests. Indeed, Yamabe and Yamazaki¹⁹ have reported a detailed theoretical study of this reaction, with important contributions for our understanding of its mechanism. They have reported a mechanism involving the dimeric Al_2Cl_6 species, rather the monomeric AlCl_3 . It is worth to say that the monomeric pathway was not analyzed, neither the dimerization equilibrium, which is critical to decide on the mechanism. In addition, they have reported that the carbon-carbon bond formation step, leading to the Wheland intermediate, is not the rate-determining one. Rather, they have found that a rearrangement of the formed product was the rate-determining step, an unexpected result. Therefore, this reaction should be investigated more deeply. Thus, the aim of this work is to perform a detailed study of the mechanism of a model Friedel-Crafts alkylation reaction and to obtain a reliable free energy profile. The system investigated is the reaction of isopropyl chloride (iPrCl) with benzene catalyzed by aluminum chloride in an apolar solvent, benzene (Scheme 2). Although many Lewis acid catalysts such as AlCl_3 , AlBr_3 , SbCl_5 , FeCl_3 , ZnCl_2 , etc. are known, the aluminum chloride is among the most active and is a classical Lewis acid for this reaction.¹¹ Because the reaction takes place in apolar medium, the different aggregates of AlCl_3 were investigated, and the solubility in benzene included in order to make an adequate comparison with experiments. It is worth to observe that classical electrophilic aromatic substitution reactions have been recently reinvestigated by reliable theoretical methods,^{22,27-37} providing more insights on these reactions.



Scheme 2. Reaction investigated in this work.

Methodology

The calculations were carried out in four steps: first, the optimized geometries of the minima and transition states (TS) were obtained using the X3LYP functional³⁸ in conjunction with the def2-SVP basis set³⁹ for C, Al and H atoms, and the ma-def2-SVP basis set⁴⁰ for the O and Cl atoms. This is a reliable functional for determining geometries.⁴¹ These geometries were characterized

as minima or transition states by harmonic frequency calculations. This calculation was also used to obtain the vibrational, rotational and translational contributions to the free energy (G_{vrt}) through the use of standard equations of statistical thermodynamics.⁴² Because we are describing reactions in condensed phase, the standard state of 1 mol L^{-1} was used to obtain the standard chemical potential in solution phase for all species by adding $1.89 \text{ kcal mol}^{-1}$ to the free energy contribution obtained from frequency calculations. The third step was performing the single point energy calculation of the electronic energies (E_{ele}) using higher level of theory, the M06-2X functional and the def2-TZVPP basis set for the C, Al and H atoms, and ma-def2-TZVPP for the atoms of O and Cl.⁴³ The M06-2X functional is a very reliable method for barrier height, staying in the top 10% best functionals in a recent benchmarking study involving 200 functionals.⁴⁴ The fourth step was determining the solvation free energy for each species (ΔG_{solv}) from the single point calculation using the continuum SMD model⁴⁵ with the X3LYP/6-31(+)-G(d) electron density (benzene solvent). The final free energy for each species in the benzene solvent (G_{sol} , $25 \text{ }^\circ\text{C}$, 1 mol L^{-1}) corresponds to a composite approach and were calculated by:

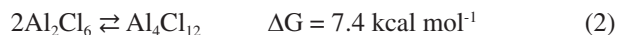
$$G_{\text{sol}} = E_{\text{ele}} + G_{\text{vrt}} + \Delta G_{\text{solv}} \quad (1)$$

In order to take advantage of the fast RIJCOSX algorithm for density functional theory computations, we have used the ORCA 3 program for geometry optimizations, harmonic frequency and single point energy calculations.⁴⁶⁻⁴⁸ The GAMESS 2016 program was used for SMD calculations because of the reliable CPCM (electrostatic part) implementation of this method.⁴⁹⁻⁵¹

Results and Discussion

Formation of $(\text{AlCl}_3)_n$ complexes

The AlCl_3 catalyst can form dimers (dim, Al_2Cl_6).^{19,52} Furthermore, it is important to evaluate the possibility of the formation of larger complexes such as trimers (trim, Al_3Cl_9), tetramers (tetram, $\text{Al}_4\text{Cl}_{12}$), and pentamers (pentam, $\text{Al}_5\text{Cl}_{15}$). In benzene, the values of the ΔG calculated for the formation of dim, trim, tetram, and pentam are equal to -16.77 , -20.60 , -26.14 , and $-29.88 \text{ kcal mol}^{-1}$, respectively (Table S1, Supplementary Information (SI) section). The ΔG for formation of these aggregates for each monomeric unit is equal to -8.38 , -6.87 , -6.53 , and $-5.98 \text{ kcal mol}^{-1}$, respectively. Thus, stabilization for each monomer unit is greater for the dim. To make this point clear, the formation of tetramer from dimer can be written as:



Therefore, aggregates larger than the dimer can be formed in a small proportion and only AlCl_3 and Al_2Cl_6 were considered in the description of the reaction mechanism in this work. The predominance of the dimer in solution phase is in agreement with experiments.⁵²

AlCl_3 catalyzed reaction

In this process, we have considered the initial Al_2Cl_6 species as reference, because the monomer is less stable. In this analysis, we have used ΔG for each step (process) and also taking the initial reactants as reference (relative). Thus, the free energy profile in the Figure 1 points out that the monomer is 8.4 kcal mol⁻¹ above of the dimer. The monomeric AlCl_3 species can interact with benzene (BZ), forming the BZ- AlCl_3 complex. The value of ΔG referring to this process is equal to -4.2 kcal mol⁻¹ (Table S1), indicating that it is less favorable than the dimerization of AlCl_3 . As a result, the ΔG of this species in the free energy profile is 4.2 kcal mol⁻¹. In the case of the complexation of AlCl_3 with *i*PrCl to form *i*PrCl- AlCl_3 , the value of ΔG for

the process is equal to -6.2 kcal mol⁻¹, also indicating that the Al_2Cl_6 dimer is more stable, because the relative ΔG for this complex becomes 2.2 kcal mol⁻¹. These results point out that in solution phase, the catalyst is present in the form of dimers and the reactants do not form stable complexes with AlCl_3 in appreciable extension.

The alkylation of benzene must occur via the previously formed *i*PrCl- AlCl_3 complex. Next, the nucleophilic attack of BZ to this complex must take place via TS1 and forming the Wheland intermediate. The ΔG^\ddagger for this step calculated in benzene is 19.6 kcal mol⁻¹. When the free energy for the *i*PrCl- AlCl_3 complex is included, the value of ΔG^\ddagger for TS1 becomes 21.8 kcal mol⁻¹. This is the effective ΔG^\ddagger barrier.

Kinetic model for monomeric AlCl_3 catalysis

The kinetic model of a reaction is useful for a correct comparison between mechanisms, because the free energy profile alone may not be enough.⁵³ Thus, consider the processes:

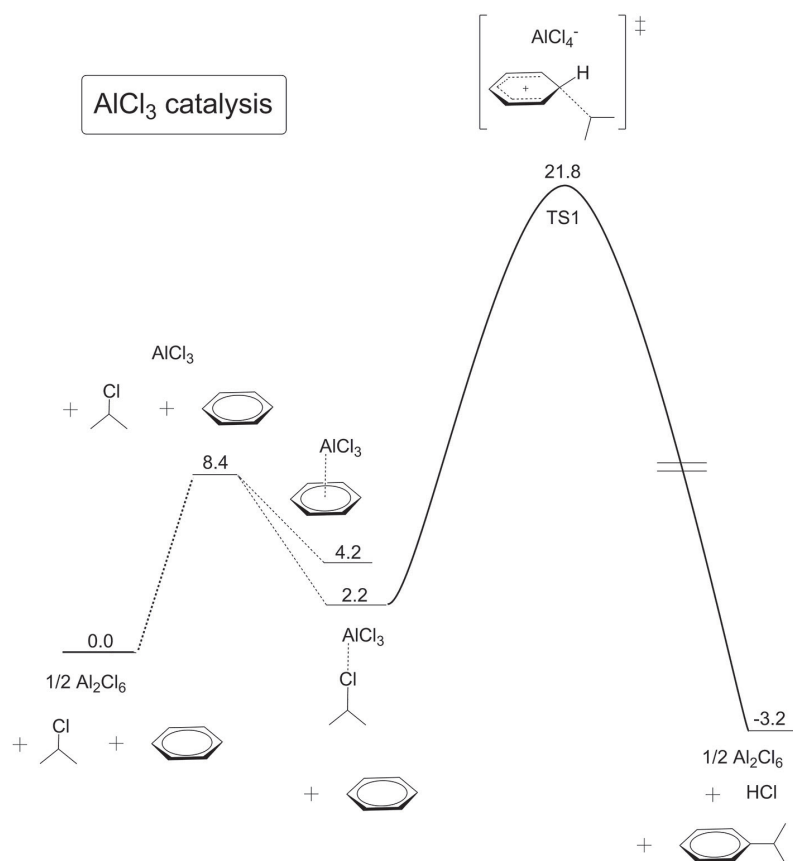


Figure 1. Free energy profile (ΔG) of the benzene alkylation reaction by isopropyl chloride using AlCl_3 as the catalytic species determined by theoretical calculations in benzene solution. Units in kcal mol⁻¹, 25 °C, and 1 mol L⁻¹ standard state. The optimized structures were obtained at X3LYP/def2-SVP level (see Figure S1 in the SI section). Single point energy calculation at M06-2X/ma-def2-TZVPP level. Wheland intermediate not included.

Equations 3 and 4 leads to the kinetic law:

$$\text{Rate} = k_{\text{obs}}[\text{Al}_2\text{Cl}_6]^{1/2}[\text{BZ}][\text{iPrCl}] \quad (5)$$

with k_{obs} related to an observed free energy barrier of:

$$\Delta G_{\text{obs}}^{\ddagger} = \Delta G_1 + \Delta G_2^{\ddagger} = 21.8 \text{ kcal mol}^{-1} \quad (6)$$

The next step is quick and involves deprotonation of the intermediate. The details of all reaction steps were done only for the case of the mechanism involving the Al_2Cl_6 , which is the most favorable reaction pathway.

The rate law in equation 6 does not take in account the solubility of the Al_2Cl_6 in benzene, which has low solubility and can limit the reaction rate. Indeed, the experimental solubility of the Al_2Cl_6 in benzene is only $3.6 \times 10^{-4} \text{ mol L}^{-1}$ at 25°C .⁵² Considering this solubility in equation 5 leads to:

$$\text{Rate} = k'_{\text{obs}}[\text{BZ}][\text{iPrCl}] \quad (7)$$

with k'_{obs} related to a new $\Delta G_{\text{obs}}^{\ddagger'} = 24.1 \text{ kcal mol}^{-1}$. This case corresponds to the use of higher amount of the catalyst, which has the reaction rate limited by its solubility.

Al_2Cl_6 catalyzed reaction

Another possible reaction pathway is the direct involvement of the Al_2Cl_6 dimer. The reaction via Al_2Cl_6 catalysis has two pathways before the nucleophilic attack of benzene: the first one involving the previous complexation of the Al_2Cl_6 dimer with BZ and iPrCl ($\text{Al}_2\text{Cl}_6 \cdot \text{iPrCl} \cdot \text{BZ}$) and the second with complexation between Al_2Cl_6 and iPrCl only ($\text{Al}_2\text{Cl}_6 \cdot \text{iPrCl}$). The calculated free energy profile is presented in the Figure 2 and the thermodynamic data are presented in Table S2 of the SI section. The values in Table S2 are considering the free species as reference, which is used in the discussion of the results. To facilitate the discussion, the processes presented in the Table S2 are numbered, and those related to the path involving $\text{Al}_2\text{Cl}_6 \cdot \text{iPrCl} \cdot \text{BZ}$ is followed by the letter “a” and those involving $\text{Al}_2\text{Cl}_6 \cdot \text{iPrCl}$ are followed by the letter “b”. These two pathways have a common intermediate, int1a1 . From this point, there is a unique pathway. Because this reaction is very complex, with some subtle changes in the structures, some steps were omitted on the Figure 2, although are presented in the Figures S1 and S2 of the SI section.

Initially, pathway “a” begins with the formation of $\text{Al}_2\text{Cl}_6 \cdot \text{iPrCl} \cdot \text{BZ}$ (process 1, Table S2) and the ΔG of this step is equal to $6.1 \text{ kcal mol}^{-1}$. It is important to note that

this complex is not the “zero” of the free energy profile, as considered by Yamabe and Yamazaki.¹⁹ Next, the int1a1 intermediate is formed with a value of relative ΔG equal to $7.80 \text{ kcal mol}^{-1}$. This intermediate is very interesting, because there is a clear C–Cl and Cl–Al bonds involving the same chlorine atom (see Figures S1 and S2 in the SI section). At the same time, only one Cl makes the bridge between the Al atoms inside the formed Al_2Cl_7^- anion. The conversion of int1a1 to int1a2 occurs via TS1a2 (process 4a, Table S2 and Figure S2, omitted in Figure 2). This transition state refers to the stretching of the C–Cl bond and a rearrangement of the complex, leading to a second ion pair, formed by the $\text{CH}_3\text{CHCH}_3^+$ carbocation and the Al_2Cl_7^- anion, interacting with the benzene. In fact, the distance of the positively charged carbon of the carbocation to a carbon of the benzene is only 2.81 \AA . The corresponding overall $\Delta G^{\ddagger} = 12.9 \text{ kcal mol}^{-1}$ for TS1a2 , an extremely low value, indicating as able the Al_2Cl_6 is for inducing the formation of the carbocation. It is worth to observe that int1a2 has $\Delta G = 13.2 \text{ kcal mol}^{-1}$, slightly above of TS1a2 , indicating that the int1a2 minima is a very shallow potential well or could not exist at all at a higher level of the theory used in the single point energy calculation. These structures, omitted from Figure 2, are not kinetically relevant.

The next step taking place is the critical one and involves the transition state TS2 , corresponding to the formation of C–C bond via nucleophilic attack of the benzene to the carbocation. The overall $\Delta G^{\ddagger} = 15.9 \text{ kcal mol}^{-1}$, the highest barrier in the free energy profile, indicating that the solubilized Al_2Cl_6 catalyst is indeed highly effective to promote the reaction. Further, it indicates that the Al_2Cl_6 species is more active than AlCl_3 , and is responsible for the catalysis. It is worth to observe that Yamabe and Yamazaki¹⁹ have not reported the step via TS2 as the highest in ΔG . Our results support the usual view that the formation of C–C bond via TS2 is the rate-determining step.

In the case of path “b”, the process is similar to path “a”. The calculations indicate higher stability of the $\text{Al}_2\text{Cl}_6 \cdot \text{iPrCl}$ than the $\text{Al}_2\text{Cl}_6 \cdot \text{iPrCl} \cdot \text{BZ}$ complex, the former being $2.7 \text{ kcal mol}^{-1}$ more stable than the latter. The reaction proceeds with the respective breaking of the Al–Cl bond, forming int1b1 , which consists of the ion pair $\text{iPr}^+ \dots \text{Al}_2\text{Cl}_7^-$. The respective transition state is TS1b1 , which is $1.4 \text{ kcal mol}^{-1}$ more stable than TS1a1 . In the next step, the int1b1 ion pair interacts with a benzene, forming the int1a1 complex. We can note that both pathways “a” and “b” that ionize the iPrCl species can take place, because the difference between the barriers referring to TS1a1 and TS1b1 is small. The next step via TS2 has the critical free energy barrier, which determines the kinetics.

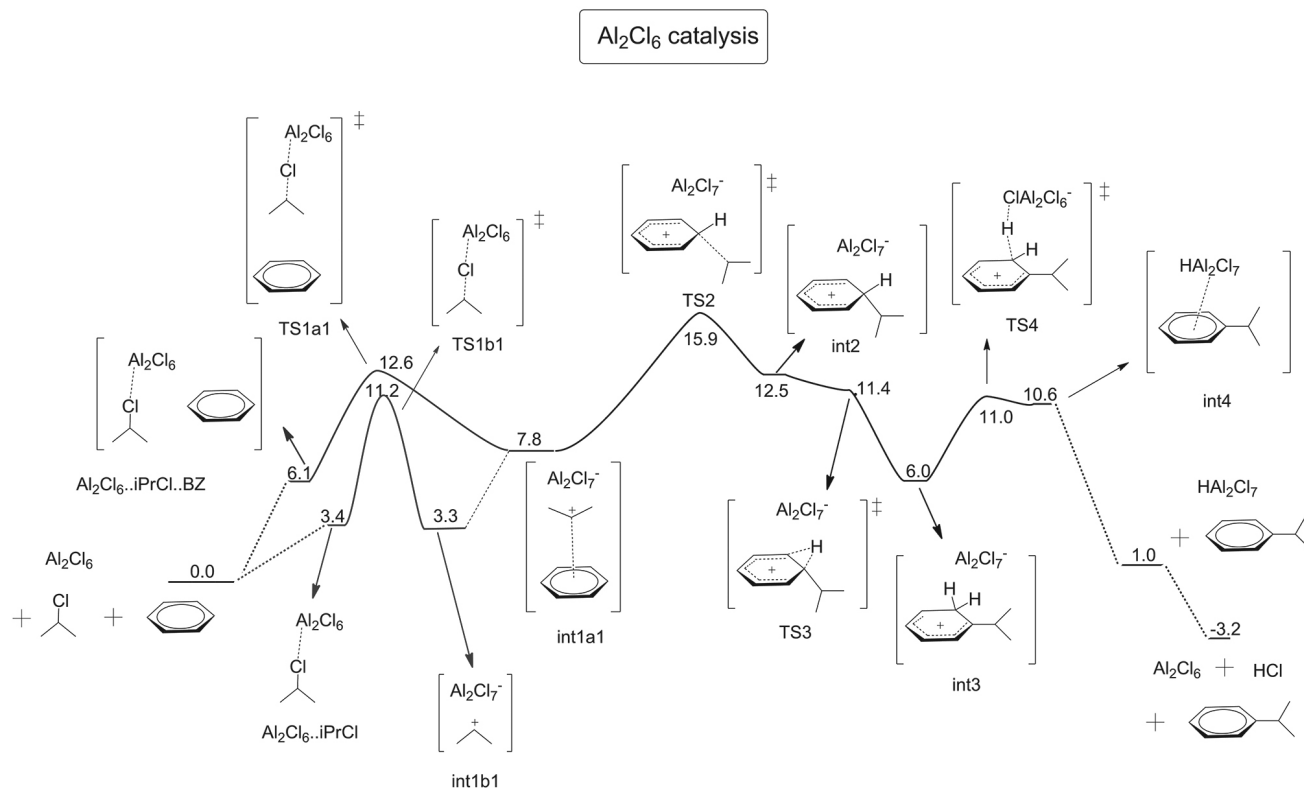


Figure 2. Free energy profile (ΔG) of the benzene alkylation reaction by isopropyl chloride using Al_2Cl_6 as the catalytic species determined by theoretical calculations in benzene solution. Units in kcal mol^{-1} , 25°C , and 1 mol L^{-1} standard state. The optimized structures were obtained at X3LYP/def2-SVP level (see Figure S1 in the SI section). Single point energy calculation at M06-2X/ma-def2-TZVPP level. Some structures were omitted for clarity. More complete mechanism in the SI section (Figure S2). Brackets were used for ion-pair and van der Waals complexes.

Once the system crosses the TS2 transition state, the intermediate int2 is formed (relative ΔG equals $12.5 \text{ kcal mol}^{-1}$, Table S2, process 7). The next step involves the migration of the proton to a vicinal carbon, and this process takes place through TS3, which has relative $\Delta G^\ddagger = 11.4 \text{ kcal mol}^{-1}$, below of int2. Again, we can note a very shallow well for int2 or even not a minimum at higher level of theory. On the other hand, the free energy profile indicates that int3 is a kinetically more stable intermediate, involving an ion pair. Finally, there is removal of the proton by the Al_2Cl_7^- species via TS4, with the respective formation of the int4. The overall ΔG^\ddagger for this transition state is $11.0 \text{ kcal mol}^{-1}$ (process 10, Table S2) and int4 has a free energy of $10.6 \text{ kcal mol}^{-1}$ (process 11, Table S2). This intermediate is a weakly bond complex between the final alkylated benzene and the HAl_2Cl_7 species. The dissociation forming a free HAl_2Cl_7 species and the alkylated product (BZiPr) leads to decrease of the free energy value to $1.0 \text{ kcal mol}^{-1}$. In the last step, the HAl_2Cl_7 species dissociates, regenerating the Al_2Cl_6 and releasing the HCl, with the value of ΔG equal to $-3.2 \text{ kcal mol}^{-1}$. Therefore, the reaction is thermodynamically favorable, although the final free energy is slightly negative. This fact indicates that to reach a high yield, the reaction should not be performed in high temperature.

Kinetic model for dimeric Al_2Cl_6 catalysis

The kinetics of the Friedel-Crafts reaction depends on the medium.⁵⁴⁻⁵⁶ Usually, this reaction takes place very quickly in solution phase and only catalytic quantities of the catalyst is needed for alkyl halide reactions catalyzed by aluminum chloride. Further, because the Al_2Cl_6 species can interact with solvents having Lewis base groups such as nitrobenzene, the kinetic law can be different in different solvents. In the present case, because the reaction takes place in low polarity benzene solution, the Al_2Cl_6 species predominates in solution phase. In addition, the experimental solubility of the Al_2Cl_6 in benzene, which is only $3.6 \times 10^{-4} \text{ mol L}^{-1}$ at 25°C ,⁵² needs be taken in account. This solubility leads to the equilibrium:



Because:

$$[\text{Al}_2\text{Cl}_6] = e^{-\Delta G_1/RT} = 3.6 \times 10^{-4} \text{ mol L}^{-1} \quad (9)$$

where T is the temperature and R the gas constant.

Based on the free energy profile of Figure 2, the reaction rate is determined by the process:



And the rate law is:

$$\text{Rate} = k_2[\text{Al}_2\text{Cl}_6][\text{BZ}][\text{iPrCl}] \quad (11)$$

with k_2 related to equation 10. This rate law corresponds to the use of the catalyst with concentration below of its solubility limit. When the solution is saturated, we can combine equations 9 and 11, which leads to the observed rate law:

$$\text{Rate} = k_{\text{obs}}[\text{BZ}][\text{iPrCl}] \quad (12)$$

with k_{obs} related to an observed free energy barrier of:

$$\Delta G_{\text{obs}}^\ddagger = \Delta G_1 + \Delta G_2^\ddagger = 20.6 \text{ kcal mol}^{-1} \quad (13)$$

This low ΔG^\ddagger corresponds to quick reaction rate in solution phase, in agreement with experimental observations of the small reaction time at room temperature for isopropyl bromide reactant.⁵⁶ The ΔG^\ddagger also agrees with longer reaction time (5 h at -6°C , 41% conversion) for the less reactive *n*-propyl chloride.¹⁰ In addition, under this low polarity condition, the system could not be homogenous, as the limited solubility of Al_2Cl_6 indicates. Thus, we have not found experimental ΔG^\ddagger for this system, only a related one in more polar, homogeneous medium.⁵⁴ Indeed, DeHaan *et al.*⁵⁴ have reported the isopropylation reaction of benzene with isopropyl chloride in nitromethane solution and have found a third order kinetics with rate constant of $5.2 \times 10^{-2} \text{ L}^2 \text{ mol}^{-2} \text{ s}^{-1}$, which translate to $\Delta G^\ddagger = 19.2 \text{ kcal mol}^{-1}$ at 25°C . Although the agreement with our value is very good, the reaction in nitromethane has a different mechanism and should involve the soluble $\text{AlCl}_3\text{-O}_2\text{NCH}_3$ complex (present in the rate law). Such polar solvent could be able to generate solvated carbocation instead of the ion pair in low polarity medium.

Conclusions

The mechanism of benzene alkylation with isopropyl chloride using the aluminum chloride as catalyst was studied in detail in apolar benzene solution using theoretical methods. A reliable free energy profile was obtained, and the calculations were followed by a kinetics analysis, including the low solubility of the catalysts. It was found that the catalyst exists as Al_2Cl_6 dimers, and this species is

the active one in the catalysis. The reaction proceeds via formation of the $\text{CH}_3\text{CHCH}_3^+ \dots \text{Al}_2\text{Cl}_7^-$ ion pair, which reacts with benzene to form the carbon-carbon bond. This step is the rate-determining one, supporting the usual view of this reaction whose kinetics is determined by the carbon-carbon bond formation step.

Supplementary Information

Supplementary data are available free of charge at <http://jbc.s bq.org.br> as PDF file.

Acknowledgments

The authors thank the agencies CNPq, FAPEMIG, and CAPES for support, and to Prof Marcelo S. Valle for the graphical art.

References

- Carey, F. A.; Sundberg, R. J.; *Advanced Organic Chemistry, Part B: Reactions and Synthesis*, 5th ed.; Springer: New York, 2007.
- Carey, F. A.; Sundberg, R. J.; *Advanced Organic Chemistry, Part A: Structure and Mechanism*, 5th ed.; Springer: New York, 2007.
- van Beurden, K.; de Koning, S.; Molendijk, D.; van Schijndel, J.; *Green Chem. Lett. Rev.* **2020**, *13*, 349. [Crossref]
- Smith, M. B.; March, J.; *March's Advanced Organic Chemistry: Reactions, Mechanisms, and Structure*; Wiley: New York, 2007.
- Sereda, G. In *Green Chemistry in Drug Discovery*; Richardson, P. F., ed.; Springer: New York, 2022, p. 155.
- Olah, G.; Reddy, V.; Prakash, G. In *Kirk-Othmer Encyclopedia of Chemical Technology*; Kirk-Othmer, ed.; John Wiley & Sons, 2000.
- Bandini, M.; Melloni, A.; Umani-Ronchi, A.; *Angew. Chem., Int. Ed. Engl.* **2004**, *43*, 550. [Crossref]
- Terrasson, V.; de Figueiredo, R. M.; Campagne, J. M.; *Eur. J. Org. Chem.* **2010**, *2010*, 2635. [Crossref]
- Heravi, M. M.; Zadsirjan, V.; Heydari, M.; Masoumi, B.; *Chem. Rec.* **2019**, *19*, 2236. [Crossref]
- Ipatieff, V. N.; Pines, H.; Schmerling, L.; *J. Org. Chem.* **1940**, *5*, 253. [Crossref]
- Price, C. C. In *Organic Reactions*; Denmark, S. E., ed.; Wiley, 2011.
- Zhang, S.; Vayer, M.; Noël, F.; Vuković, V. D.; Golushko, A.; Rezajooei, N.; Rowley, C. N.; Lebœuf, D.; Moran, J.; *Chem* **2021**, *7*, 3425. [Crossref]
- Wang, S.; Force, G.; Guillot, R.; Carpentier, J.-F.; Sarazin, Y.; Bour, C.; Gandon, V.; Lebœuf, D.; *ACS Catal.* **2020**, *10*, 10794. [Crossref]
- Chowdhury, A. D.; Houben, K.; Whiting, G. T.; Chung, S.-H.; Baldus, M.; Weckhuysen, B. M.; *Nat. Catal.* **2018**, *1*, 23. [Crossref]

15. Rueping, M.; Nachtsheim, B. J.; *Beilstein J. Org. Chem.* **2010**, *6*, 6. [Crossref]
16. Spencer, S. R.; Zhang, M.; Lund, C. R. F.; *J. Phys. Chem. A* **2003**, *107*, 10335. [Crossref]
17. Tarakeshwar, P.; Kim, K. S.; *J. Phys. Chem. A* **1999**, *103*, 9116. [Crossref]
18. Tarakeshwar, P.; Lee, J. Y.; Kim, K. S.; *J. Phys. Chem. A* **1998**, *102*, 2253. [Crossref]
19. Yamabe, S.; Yamazaki, S.; *J. Phys. Org. Chem.* **2009**, *22*, 1094. [Crossref]
20. Corma, A.; Garcia, H.; *Chem. Rev.* **2003**, *103*, 4307. [Crossref]
21. Melissen, S. T.; Tognetti, V.; Dupas, G.; Jouanneau, J.; Lê, G.; Joubert, L.; *J. Mol. Model.* **2013**, *19*, 4947. [Crossref]
22. de Queiroz, J. F.; Carneiro, J. W. M.; Sabino, A. A.; Sparrapan, R.; Eberlin, M. N.; Esteves, P. M.; *J. Org. Chem.* **2006**, *71*, 6192. [Crossref]
23. Borisov, Y. A.; Akhrem, I. S.; *Mol. Catal.* **2020**, *482*, 100300. [Crossref]
24. Volkov, A. N.; Timoshkin, A. Y.; Suvorov, A. V.; *Int. J. Quantum Chem.* **2005**, *104*, 256. [Crossref]
25. Volkov, A. N.; Timoshkin, A. Y.; Suvorov, A. V.; *Int. J. Quantum Chem.* **2004**, *100*, 412. [Crossref]
26. Oliveira, F. G.; Rodrigues, F. L.; de Oliveira, A. V. B.; Marçal, D. V. L. M.; Esteves, P. M.; *Struct. Chem.* **2017**, *28*, 545. [Crossref]
27. Pliego Jr., J. R.; *Comput. Theor. Chem.* **2021**, *1198*, 113171. [Crossref]
28. Shernyukov, A. V.; Genaev, A. M.; Salnikov, G. E.; Shubin, V. G.; Rzepa, H. S.; *Org. Biomol. Chem.* **2019**, *17*, 3781. [Crossref]
29. Liljenberg, M.; Stenlid, J. H.; Brinck, T.; *J. Phys. Chem. A* **2018**, *122*, 3270. [Crossref]
30. Shernyukov, A. V.; Genaev, A. M.; Salnikov, G. E.; Rzepa, H. S.; Shubin, V. G.; *J. Comput. Chem.* **2016**, *37*, 210. [Crossref]
31. Galabov, B.; Nalbantova, D.; Schleyer, P. v. R.; Schaefer, H. F.; *Acc. Chem. Res.* **2016**, *49*, 1191. [Crossref]
32. Galabov, B.; Koleva, G.; Simova, S.; Hadjieva, B.; Schaefer, H. F.; Schleyer, P. v. R.; *Proc. Natl. Acad. Sci.* **2014**, *111*, 10067. [Crossref]
33. Galabov, B.; Koleva, G.; Kong, J.; Schaefer III, H. F.; Schleyer, P. v. R.; *Eur. J. Org. Chem.* **2014**, *2014*, 6918. [Crossref]
34. Kong, J.; Galabov, B.; Koleva, G.; Zou, J.-J.; Schaefer III, H. F.; Schleyer, P. v. R.; *Angew. Chem., Int. Ed.* **2011**, *50*, 6809. [Crossref]
35. Liljenberg, M.; Stenlid, J. H.; Brinck, T.; *J. Mol. Model.* **2017**, *24*, 15. [Crossref]
36. Koleva, G.; Galabov, B.; Hadjieva, B.; Schaefer III, H. F.; Schleyer, P. v. R.; *Angew. Chem., Int. Ed.* **2015**, *54*, 14123. [Crossref]
37. Parker, V. D.; Kar, T.; Bethell, D.; *J. Org. Chem.* **2013**, *78*, 9522. [Crossref]
38. Xu, X.; Zhang, Q.; Muller, R. P.; Goddard III, W. A.; *J. Chem. Phys.* **2005**, *122*, 14105. [Crossref]
39. Weigend, F.; Ahlrichs, R.; *Phys. Chem. Chem. Phys.* **2005**, *7*, 3297. [Crossref]
40. Zheng, J.; Xu, X.; Truhlar, D. G.; *Theor. Chem. Acc.* **2011**, *128*, 295. [Crossref]
41. Brémond, É.; Savarese, M.; Su, N. Q.; Pérez-Jiménez, Á. J.; Xu, X.; Sancho-García, J. C.; Adamo, C.; *J. Chem. Theory Comput.* **2016**, *12*, 459. [Crossref]
42. McQuarrie, D.; *Statistical Mechanics*; University Science Books: Sausalito, CA, 2000.
43. Zhao, Y.; Truhlar, D. G.; *Theor. Chem. Acc.* **2008**, *120*, 215. [Crossref]
44. Mardirossian, N.; Head-Gordon, M.; *Mol. Phys.* **2017**, *115*, 2315. [Crossref]
45. Marenich, A. V.; Cramer, C. J.; Truhlar, D. G.; *J. Phys. Chem. B* **2009**, *113*, 6378. [Crossref]
46. Neese, F.; *Wiley Interdiscip. Rev.: Comput. Mol. Sci.* **2012**, *2*, 73. [Crossref]
47. Neese, F.; Wennmohs, F.; Becker, U.; Riplinger, C.; *J. Chem. Phys.* **2020**, *152*, 224108. [Crossref]
48. Neese, F.; *ORCA: an ab initio, DFT and semiempirical SCF-MO package*; version: 3.0.3; Max-Planck-Institute for Chemical Energy Conversion, Germany, 2013.
49. Barca, G. M. J.; Bertoni, C.; Carrington, L.; Datta, D.; de Silva, N.; Deustua, J. E.; Fedorov, D. G.; Gour, J. R.; Gunina, A. O.; Guidez, E.; Harville, T.; Irle, S.; Ivanic, J.; Kowalski, K.; Leang, S. S.; Li, H.; Li, W.; Lutz, J. J.; Magoulas, I.; Mato, J.; Mironov, V.; Nakata, H.; Pham, B. Q.; Piecuch, P.; Poole, D.; Pruitt, S. R.; Rendell, A. P.; Roskop, L. B.; Ruedenberg, K.; Sattasathuchana, T.; Schmidt, M. W.; Shen, J.; Slipchenko, L.; Sosonkina, M.; Sundriyal, V.; Tiwari, A.; Galvez Vallejo, J. L.; Westheimer, B.; Wloch, M.; Xu, P.; Zahariev, F.; Gordon, M. S.; *J. Chem. Phys.* **2020**, *152*, 154102. [Crossref]
50. Schmidt, M. W.; Baldridge, K. K.; Boatz, J. A.; Elbert, S. T.; Gordon, M. S.; Jensen, J. H.; Koseki, S.; Matsunaga, N.; Nguyen, K. A.; Su, S.; Windus, T. L.; Dupuis, M.; Montgomery, J. A.; *J. Comput. Chem.* **1993**, *14*, 1347. [Crossref]
51. Gordon, M. S.; Schmidt, M. W.; *GAMESS: General Atomic and Molecular Electronic Structure System*; Iowa State University, USA, 2016.
52. Eley, D.; King, P.; *Trans. Faraday Soc.* **1951**, *47*, 1287. [Crossref]
53. Pliego, J. R.; *J. Organomet. Chem.* **2022**, *973-974*, 122397. [Crossref]
54. DeHaan, F. P.; Delker, G. L.; Covey, W. D.; Ahn, J.; Cowan, R. L.; Fong, C. H.; Kim, G. Y.; Kumar, A.; Roberts, M. P.; *J. Org. Chem.* **1986**, *51*, 1587. [Crossref]
55. Carter, B. J.; Covey, W. D.; DeHaan, F. P.; *J. Am. Chem. Soc.* **1975**, *97*, 4783. [Crossref]
56. Olah, G. A.; Flood, S. H.; Kuhn, S. J.; Moffatt, M. E.; Overchuck, N. A.; *J. Am. Chem. Soc.* **1964**, *86*, 1046. [Crossref]

Submitted: May 9, 2022

Published online: July 14, 2022

